Inorg. Chem. **2008**, *47*, 2416−2427

Reactivity and Spectroscopy of the {Ru(DMAP)$_5$} Fragment: An {Ru(NH$_3$)$_5$} Analogue

Melina B. Rossi,[†] Oscar E. Piro,[‡] Eduardo E. Castellano,[§] Pablo Alborés,*[,†] and Luis M. Baraldo*[,†]

Departamento de Química Inorgánica, Analítica y Química Física, INQUIMAE, Facultad de Ciencias Exactas y Naturales Universidad de Buenos Aires, Pabellón 2, Ciudad Universitaria, C1428EHA Buenos Aires, Argentina, Departamento de Física, Facultad Ciencias Exactas, Universidad Nacional de La Plata and IFLP (CONICET), CC 67, 1900 La Plata, Argentina, and Instituto de Física de São Carlos, Universidade de São Pablo, CP. 369, 13560 São Carlos (SP), Brazil

Received August 17, 2007

Reaction of *trans*-Ru(DMSO)$_4$Cl$_2$ with DMAP (DMAP = 4-dimethylaminopyridine) yields the yellow [Ru(DMAP)$_6$]$^{2+}$ cation in good yield. The crystal and molecular structure of [Ru(DMAP)$_6$]Cl$_2$·6CH$_3$CH$_2$OH was determined by X-ray diffraction methods. The complex crystallizes in the trigonal $R\bar{3}$ space group with $a = b = 16.373(1)$, $c = 20.311(1)$ Å, $\gamma = 120°$, and $Z = 3$ molecules per unit cell. The reaction of [Ru(DMAP)$_6$]$^{2+}$ in aerobic water gives the red [Ru^{III}(DMAP)$_5$(OH)]$^{2+}$ cation. This complex shows a chemical behavior similar to [Ru^{III}(NH$_3$)$_5$Cl]$^{2+}$ and allows the preparation of a family of [Ru(DMAP)$_5$L]$^{n+}$ complexes. Their electronic properties indicate that the {Ru^{II}(DMAP)$_5$} fragment is a weaker π-donor than {Ru^{II}(NH$_3$)$_5$}. Our density functional theory (DFT) calculations show that in {Ru^{II}(DMAP)$_5$} the DMAP ligands can compete for the π electron density of the ruthenium making the fragment a weaker π-donor.

Introduction

Among the large number of ruthenium-based building blocks reported in the literature, the {Ru(NH$_3$)$_5$} fragment[1] is undoubtedly one of the more explored, mainly due to its widespread use in the synthesis of binuclear, trinuclear, and supramolecular transition metal-containing complexes,[2] the Creutz−Taube dimer being probably the most famous example of this chemistry.[3]

With the aim of exploring new electron-rich ruthenium fragments, we investigated the reaction of *trans*-Ru(DMSO)$_4$Cl$_2$ with the highly basic (pK_a = 9.7[4]) 4-dimethylaminopyridine ligand (DMAP). Known antecedents of this reaction refer exclusively to the preparation of neutral *trans*-Ru(L)$_4$Cl$_2$ compounds with L being a substituted pyridine ligand.[5,6] Surprisingly enough, the reaction produced the hexa-substituted [Ru(DMAP)$_6$]$^{2+}$ complex in high yield instead of the expected *trans*-Ru(DMAP)$_4$Cl$_2$ compound, as revealed by the crystal structure of its chloride salt. This one-pot reaction clearly contrasts with the synthesis of the related [Ru(py)$_6$]$^{2+}$ complex which requires several steps.[7]

The exploration of the reactivity exhibited by this novel Ru(II) precursor revealed that under aerobic aqueous conditions it readily converts to the [Ru^{III}(DMAP)$_5$(OH)]$^{2+}$ ion, whose chemistry nicely mirrors that of the [Ru(NH$_3$)$_5$Cl]$^{2+}$

* Corresponding authors. E-mail: albores@qi.fcen.uba.ar (P.A.); baraldo@qi.fcen.uba.ar (L.M.B.).
[†] Facultad de Ciencias Exactas y Naturales Universidad de Buenos Aires.
[‡] Universidad Nacional de La Plata and IFLP (CONICET).
[§] Universidade de São Pablo.

(1) Taube, H. *Pure Appl. Chem.;* **1979**, *51*, 901.
(2) (a) Watzky, M. A.; Macatangay, A. V.; VanCamp, R. A.; Mazzetto, S. E.; Song, X. Q.; Endicott, J. F.; Buranda, T. *J. Phys. Chem. A* **1997**, *101*, 8441. (b) Watzky, M. A.; Endicott, J. F.; Song, X. Q.; Lei, Y. B.; Macatangay, A. *Inorg. Chem.* **1996**, *35*, 3463. (c) Sommovigo, M.; Ferretti, A.; Venturi, M.; Ceroni, P.; Giardi, C.; Denti, G. *Inorg. Chem.* **2002**, *41*, 1263. (d) Scandola, F.; Argazzi, R.; Bignozzi, C. A.; Chiorboli, C.; Indelli, M. T.; Rampi, M. A. *Coord. Chem. Rev.* **1993**, *125*, 283. (e) Moscherosch, M.; Waldhor, E.; Binder, H.; Kaim, W.; Fiedler, J. *Inorg. Chem.* **1995**, *34*, 4326. (f) Macatangay, A. V.; Endicott, J. F. *Inorg. Chem.* **2000**, *39*, 437. (g) Bignozzi, C. A.; Argazzi, R.; Schoonover, J. R.; Gordon, K. C.; Dyer, R. B.; Scandola, F. *Inorg. Chem.* **1992**, *31*, 5260.
(3) Creutz, C.; Taube, H. *J. Am. Chem. Soc.* **1969**, *91*, 3988.
(4) *CRC Handbook of Chemistry and Physics*, 81st ed.; Lide, D. R., Ed.; CRC Press: Boca Raton, FL, 1995; p 2000.
(5) Albores, P.; Slep, L. D.; Weyhermuller, T.; Baraldo, L. M. *Inorg. Chem.* **2004**, *43*, 6762.
(6) Evans, I. P.; Spencer, A.; Wilkinson, G .*J. Chem. Soc., Dalton Trans.* **1973**, 204.
(7) Templeton, J. L. *J. Am. Chem. Soc.* **1979**, *101*, 4906.

10.1021/ic7016352 CCC: $40.75
Published on Web 03/13/2008

moiety.[8] We have studied the aqueous redox chemistry of this complex and found that the Ru(IV) redox state is readily accessible and gives rise to the Ru(IV) oxo species as the only product. The $[Ru^{III}(DMAP)_5(OH)]^{2+}$ ion can also be easily reduced yielding the labile $[Ru^{II}(DMAP)_5(OH_2)]^{2+}$ species that allows the preparation of a family of $[Ru(DMAP)_5L]^{n+}$ compounds, whose spectroscopic and electrochemical properties are reported here. These complexes resemble their $\{Ru(NH_3)_5\}$ analogues but show evidence of a less significant electronic coupling between the ruthenium and the sixth ligand.

Experimental Section

Materials. The complex *trans*-$[Ru(DMSO)_4Cl_2]$[6] and the ligand *N*-methylpyrazinium iodide (MepzI)[9] were prepared following previously reported techniques. Solvents for UV–visible and electrochemistry measurements were dried according to literature procedures. All other reagents were obtained commercially and used as supplied. All the compounds synthesized in this work were dried in a vacuum desiccator for at least 12 h prior to characterization.

Synthesis of the Complexes. $[Ru(DMAP)_6]Cl_2\cdot 9H_2O$ (1). A 23 g portion of 4-dimethylaminopyridine was partially dissolved in 100 mL of ethanol and 2.3 g of *trans*-$Ru(DMSO)_4Cl_2$ was added. The suspension was deoxygenated by argon bubbling and refluxed while stirring under argon atmosphere for 4 h. The final orange solution was cooled to rt and 500 mL of diethyl ether were added under an argon stream. A light yellow solid immediately appeared and was collected by filtration, washed thoroughly with diethyl ether, dried in vacuum, and kept protected from air moisture. Single crystals of **1** suitable for structural X-ray diffraction studies were grown by slow diethyl ether diffusion at low temperature into an ethanol solution of the salt. Yield: 85%. Anal. Calcd. for $C_{42}H_{60}Cl_2N_{12}Ru\cdot 9H_2O$: C, 47.3; H, 7.4; N, 15.8. Found: C, 48.0; H, 7.0; N, 15.7. δ_H (CCl_3D) 7.46 (12H, d, H_{orto}), 6.51 (12H d, H_{meta}), 3.07 (36H, s, $H_{methyls}$). IR ($C-N(CH_3)_2$) ν: 1620 cm^{-1}.

$[Ru(DMAP)_6][PF_6]_3$ (2). A 0.105 g portion of **1** was dissolved in ca. 10 mL of acetonitrile and 0.056 g of solid $[NH_4]_2[Ce(NO_3)_6]$ were added. The solution turned blue immediately, and a solid appeared. The latter was redissolved by the addition of 10 mL of water. The resulting solution was rotoevaporated until a few milliliters of water remained. After addition of solid KPF_6, the desired product precipitated. The solid was filtered off, washed with water, and vacuum-dried (0.111 g, yield 89%). *Note:* similar results were obtained precipitating the product with $NaClO_4$. Anal. Calcd. for $C_{42}H_{60}N_{12}P_3F_{18}Ru$: C, 39.8; H, 4.7; N, 13.2. Found: C, 40.3; H, 4.9; N, 12.9. IR ($C-N(CH_3)_2$) ν: 1621 cm^{-1}. **Caution!** *Perchlorate salts of metal complexes with organic ligands are often explosive. Although we have had no problems with the perchlorate salts described in this work, such compounds should be handled with great caution.*

$[Ru(DMAP)_5(OH)][ClO_4]_2\cdot 1.5H_2O$ (3). A 1 g portion of complex **1** was dissolved in 40 mL of distilled water. The orange solution was heated to 40 °C while stirring over ca. 3 h until complete conversion of the UV–vis spectrum. To the resulting deep purple solution, solid $NaClO_4$ was added until almost complete precipitation of the product. The latter was filtered, washed with cold water, and vacuum-dried. Yield: 0.761 g, 85% Anal. Calcd. for $C_{35}H_{51}N_{10}O_9Cl_2Ru\cdot 1.5H_2O$: C, 44.0; H, 5.7; N, 14.7. Found: C, 44.4; H, 5.5; N, 14.8. IR ($C-N(CH_3)_2$) ν: 1622 cm^{-1}. *Note*: the same procedure, but with addition of KPF_6 instead of $NaClO_4$, afforded the PF_6 salt. For the preparation of the chloride salt, instead of addition of $NaClO_4$, the solution was evaporated to dryness. The resulting solid was washed with diethyl ether to remove the free DMAP ligand and then dried in vacuo.

$[Ru(DMAP)_5(OH_2)][PF_6]_3\cdot 1.5H_2O$ (4). A 0.025 g portion of the chloride salt of complex **3** was dissolved in 2.5 mL of water. This solution was acidified with HCl 1 M until pH ca. 3, obtaining a deep blue solution. A saturated aqueous solution of NH_4PF_6 was added until complete precipitation of the desired product. The solid was filtrated, washed with cold water, and vacuum-dried. Yield: 0.024 g, 70%. *Note*: addition of $NaClO_4$ instead of NH_4PF_6 allowed the production of the perchlorate salt.

$[Ru(DMAP)_5(O)][ClO_4]_2\cdot 1.5H_2O$ (5). The chloride salt of complex **3** was dissolved in water, and a hypochlorite solution was dropwise added. The solution turned immediately brownish yellow. Solid $NaClO_4$ was added until complete precipitation of the desired product. This solid was filtered, washed with cold water, vacuum-dried, and stored under an argon atmosphere at 0 °C where it decomposed in ca. 2–3 h yielding the Ru(III) hydroxo species. IR ($C-N(CH_3)_2$) ν: 1624 cm^{-1}, (Ru−O) ν: 812 cm^{-1}. μ_{eff} (μ_B) 298 K: 3.09. Anal. Calcd. for $C_{35}H_{50}N_{10}O_9Cl_2Ru\cdot 1.5H_2O$: C, 44.1; H, 5.6; N, 14.7. Found: C, 44.3; H, 5.0; N, 13.6 Reactivity experiments, magnetic measurements, and spectroscopic determinations were carried out before decomposition of the solid compound.

$[Ru(DMAP)_5(Mepz)][PF_6]_3\cdot 4H_2O$ (6). A solution of $MepzNO_3$ was prepared by dissolution of 8 g of MepzI in a minimum amount of water followed by the addition of 0.2 g of $AgNO_3$. The solid AgI was removed by filtration obtaining a clear solution of the $Mepz^+$ nitrate salt which was deareated by argon bubbling. The chloride salt of complex **3** (0.1 g) was dissolved in 25 mL of deoxygenated water, and some Zn(Hg) pieces were added. This solution was stirred under an argon atmosphere until the solution turned from purple to a yellow color. At this point, the solution was anaerobically transferred to the $Mepz^+$ solution, and the resulting mixture was stirred under argon atmosphere for 20 h. The resulting blue solution obtained was filtered, and solid NH_4PF_6 was added until complete precipitation of the product. The solid was filtered, washed with cold water, and vacuum-dried. Yield: 0.053 g, 32%. Anal. Calcd. for $C_{40}H_{57}N_{12}P_3F_{18}Ru\cdot 4H_2O$: C, 36.5; H, 4.9; N, 12.8. Found: C, 36.8; H, 4.2; N, 13.1. δ_H (CD_3OD) 9.12 (2H, d, H_{orto}Mepz), 8.29 (2H d, H_{meta}Mepz), 7.53 (2H, d, $H_{orto}DMAP_{ax}$), 7.43 (8H d, $H_{orto}DMAP_{eq}$), 6.76 (2H d, $H_{meta}DMAP_{ax}$), 6.67 (8H d, $H_{meta}DMAP_{eq}$), 6.21 (3H s, H_{methyl} Mepz), 3.12 (6H s, $H_{methyl}DMAP_{ax}$), 3.07 (24H s, $H_{methyl}DMAP_{eq}$). IR ($C-N(CH_3)_2$) ν: 1624 cm^{-1}.

In situ Preparation of $[Ru(DMAP)_5(pz)]^{2+}$. The same procedure as for the synthesis of compound **6** was carried out for the preparation of an aqueous solution of $[Ru(DMAP)_5(pz)]^{2+}$. A 10-fold excess of pyrazine was used, and the reaction time was 4 h. Our efforts to isolate the perchlorate or hexafluorophosphate salt from this complex were unsuccessful, as the resulting solid quickly decomposes.

Physical Measurements. IR spectra were collected on KBr pellets with a Nicolet FTIR 510P instrument. UV–visible spectra were recorded in the range between 190 and 1100 nm with a Hewlett-Packard 8453 diode array spectrometer. Elemental analyses were performed with a Carlo Erba 1108 analyzer. Hydration water molecules in the reported complexes were determined by thermogravimetric measurements with a TGA-51 Shimadzu thermogravimetric analyzer. NMR spectra were obtained with a Bruker AM-500 spectrometer. Cyclic voltam-

(8) Ford, P.; Rudd, D. F. P.; Gaunder, R.; Taube, H. *J. Am. Chem. Soc.* **1968**, *90*, 1187.
(9) Koelsch, C. F.; Gumprecht, W. H. *J. Org. Chem.* **1958**, *23*, 1603.

metry measurements were carried out under argon with millimolar solutions of the compounds, using a PAR 273A potensiostat and a standard three electrode arrangement consisting of a glassy carbon disk (area = 9.4 mm^2) as the working electrode, a platinum wire as the counter electrode, and a reference electrode. Depending on the situation, the latter was an Ag/AgCl 3 M KCl standard electrode (for aqueous solutions) or a silver wire plus an internal standard (ferrocene) for organic solvents. KNO_3 1 M and tetra-*n*-butylammonium hexaflourophosphate ($TBAPF_6$) 0.1 M were used as supporting electrolytes in water and nonaqueous media, respectively. For the pH dependence measurements of complex **3** redox potentials, the buffer solutions provided adequate ionic strength. All the potentials reported in this work are referenced to the standard Ag/AgCl saturated KCl electrode (0.197 V vs normal hydrogen electrode (NHE)). Spectroelectrochemical measurements were performed with an optically transparent thin layer electrode cell (OTTLE) equipped with two 4 × 2 mm CaF_2 windows (with about 0.2 mm of path length), a working Pt electrode grid (0.25 mm^2), a Pt counter electrode grid (0.5 mm^2), and an Ag wire reference electrode. KNO_3 0.1 M or $TBAPF_6$ 0.1 M were used as supporting electrolytes. pH measurements were carried out with a Metrohm 744 pHmeter calibrated with standard buffer solutions. Magnetic moment measurements of solid samples at room temperature were performed with a Johnson Matthey magnetic susceptibility balance (MSB) with a $MnSO_4$ aqueous solution as a reference. The diamagnetic contribution was subtracted using Pascal's formula.

Crystal Data, X-ray Data Collection, and Structure Solution and Refinement. The crystals were stable while kept in their mother solution. To prevent their degradation during data collection, a single-crystal was soaked in a synthetic oil drop and mounted on top of a glass fiber. The sample was then cooled down to low temperature by blowing boiling nitrogen vapor with a cryostat device attached to the X-ray apparatus. Diffraction data were collected on an Enraf-Nonius Kappa CCD diffractometer (employing φ and ω scans) with COLLECT[10] and reduced with the DENZO and SCALEPACK[11] programs. The data were corrected empirically for absorption with PLATON.[12] The structure was solved by direct and Fourier methods with the SHELXS[13] program, and its non-H atoms were refined by full-matrix least-squares with the SHELXL[14] program. The hydrogen atoms were located stereochemically and refined with the riding model. The ligand methyl hydrogen positions and those of the EtOH solvent molecule were optimized by treating the groups as rigid and allowing them to rotate during the refinement around the corresponding C−N and C−C bonds. Crystal data and refinement results are summarized in Table 1. Crystallographic data (excluding structure factors) have been deposited with the Cambridge Crystallographic Data Centre as supplementary publication no. CCDC 643466. Copies of the data can be obtained free of charge upon application to CCDC, 12 Union Road, Cambridge CB2 1EZ, U.K. (Fax: (44) 1223 336-033. E-mail: deposit@ccdc.cam.ac.uk).

Table 1. Crystal Data and Structure Refinement Results for $[Ru(DMAP)_6]Cl_2 \cdot 6CH_3CH_2OH$

empirical formula	$C_{54}H_{96}Cl_2N_{12}O_6Ru$
formula weight	1181.40
temperature (K)	100(2)
crystal system	trigonal
space group	$R\bar{3}$ (No. 148)
unit cell dimensions[a]	
$a = b$ (Å)	16.373(1)
c (Å)	20.311(1)
γ (deg)	120.00
volume (Å^3)	4715.4(5)
Z, calculated density (Mg/m^3)	3, 1.248
absorption coefficient (mm^{-1})	0.389
F(000)	1890
crystal size (mm)	0.18 × 0.18 × 0.12
crystal color/shape	red/fragment
radiation, graphite monochromator	Mo Kα, $\lambda = 0.71073$ Å
θ range data collection (deg)	3.04 to 26.00
index ranges	$-20 \le h \le 20$, $-20 \le k \le 19$, $-25 \le l \le 25$
reflections collected/unique	10694/2056 [R(int) = 0.0309]
observed reflections [$I > 2\sigma(I)$]	1952
completeness (%)	99.7 (to $\theta = 26.00°$)
max and min transmission	0.983 and 0.930
refinement method	full-matrix least-squares on F^2
weights, w	$[\sigma^2(F_o^2) + (0.034P)^2 + 10.15P]^{-1}$ $P = [\max(F_o^2,0) + 2F_c^2]/3$
data/restraints/parameters	2056/0/118
goodness-of-fit on F^2	1.088
final R-index [$I > 2\sigma(I)$][b]	$R_1 = 0.0292$, $wR_2 = 0.0761$
R indices (all data)	$R_1 = 0.0312$, $wR_2 = 0.0780$
largest peak and hole (e/A^3)	0.381 and −0.642

[a] Least-squares refinement of the angular settings for 10694 reflections in the $3.04 < \theta < 26.00°$ range. [b] R-indices defined as: $R_1 = \Sigma||F_o| - |F_c||/\Sigma|F_o|$, $wR_2 = [\Sigma w(F_o^2 - F_c^2)^2/\Sigma w(F_o^2)^2]^{1/2}$.

Theoretical Calculations. We employed density functional theory (DFT) computations to fully optimize the geometries of the reported complexes, without symmetry constraints. The calculations were performed with Gaussian 03,[15] at the B3LYP level, employing the LanL2DZ basis set, which proved to be suitable for geometry predictions in coordination compounds containing metals of the first and second rows of transition elements in the periodic table. We used tight self-consistent-field convergence criteria and default settings in the geometry optimizations. For the closed-shell compounds and the ones with an odd number of electrons, restricted and unrestricted approximations of the Kohn–Sham equations were used, respectively. Time-dependent, TD-DFT, computation at the equilibrium geometry was calculated to assist in the interpretation and assignment of the electronic spectra. Infrared frequencies were calculated for the $[Ru(DMAP)_5(OH)]^{2+}$ and $[Ru(DMAP)_5O]^{2+}$ complexes to confirm the assignment of the Ru^{IV}═O stretching

(10) Enraf-Nonius, B. V. *COLLECT data collection software*; Nonius BV, Delft, The Netherlands; 1997–2000.

(11) Otwinowski, Z.; Minor, W. In *Methods in Enzymology: Macromolecular Crystallography*; Carter, C. W., Sweet, R. M., Eds.; Academic Press: San Diego, 1997; Vol. *276*, p 307.

(12) Spek, A. L. *PLATON, A Multipurpose Crystallographic Tool*; Utrecht University: Utrecht, The Netherlands, 2000.

(13) Sheldrick, G. M. *SHELXS-97. Program for Crystal Structure Resolution*; University of Göttingen: Göttingen, Germany, 1997.

(14) Sheldrick, G. M. *SHELXL-97. Program for Crystal Structures Analysis*; University of Göttingen: Göttingen, Germany, 1997.

(15) Frisch, M. J.; Trucks, G. W.; Schlegel, H. B.; Scuseria, G. E.; Robb, M. A.; Cheeseman, J. R.; Montgomery, J. A.; Vreven, T., Jr.; Kudin, K. N.; Burant, J. C.; Millam, J. M.; Iyengar, S. S.; Tomasi, J.; Barone, V.; Mennucci, B.; Cossi, M.; Scalmani, G.; Rega, N.; Petersson, G. A.; Nakatsuji, H.; Hada, M.; Ehara, M.; Toyota, K.; Fukuda, R.; Hasegawa, J.; Ishida, M.; Nakajima, T.; Honda, Y.; Kitao, O.; Nakai, H.; Klene, M.; Li, X.; Knox, J. E.; Hratchian, H. P. Cross, J. B.; Adamo, C.; Jaramillo, J.; Gomperts, R.; Stratmann, R. E.; Yazyev, O.; Austin, A. J.; Cammi, R.; Pomelli, C.; Ochterski, J. W.; Ayala, P. Y.; Morokuma, K.; Voth, G. A.; Salvador, P.; Dannenberg, J. J.; Zakrzewski, V. G.; Dapprich, S.; Daniels, A. D.; Strain, M. C.; Farkas, O.; Malick, D. K.; Rabuck, A. D.; Raghavachari, K.; Foresman, J. B.; Ortiz, J. V.; Cui, Q.; Baboul, A. G.; Clifford, S.; Cioslowski, J.; Stefanov, B. B.; Liu, G.; Liashenko, A.; Piskorz, P.; Komaromi, I.; Martin, R. L.; Fox, D. J.; Keith, T.; Al-Laham, M. A.; Peng, C. Y.; Nanayakkara, A.; Challacombe, M.; Gill, P. M. W.; Johnson, B.; Chen, W.; Wong, M. W.; Gonzalez, C.; Pople, J. A. *Gaussian 03*; Gaussian Inc.: Wallingford, CT, 2003.

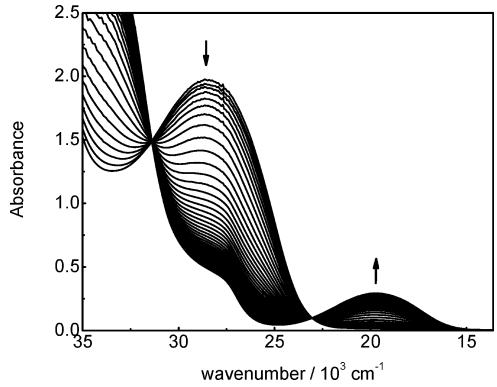

Figure 1. UV–vis spectrophotometrical monitoring of the reaction involving $[Ru(DMAP)_6]^{2+}$ in aerated water solution. Arrows indicate the temporal evolution of the bands.

band. For the latter compound, a spin multiplicity of 3 (S = 1) was used as expected for a d^4 ion in the presence of the strong π donor oxo ligand.

pK_a Determinations. The pK_a values for the protonation of the coordinated pyrazine in $[Ru(DMAP)_5pz]^{2+}$ and for the protonation of $[Ru(DMAP)_5(OH)]^{2+}$ were obtained measuring its UV–vis spectra in 0.1 M $H_3PO_4/H_2PO_4^-$ or 0.1 M CH_3COOH/CH_3COO^- buffer solutions in the 0.0–2.5 and in the 4.0–7.7 pH range, respectively.

Acid–Base Titration of $[Ru(DMAP)_5(OH)]^{2+}$. Titration of the acid–base equivalents of $[Ru(DMAP)_5(OH)]^{2+}$ was performed using valorated HCl solutions. The progress of the neutralization reaction was monitored by UV–vis spectrophotometric measurements.

Results

Synthetic Procedures. Reaction of *trans*-$Ru(DMSO)_4Cl_2$ in absolute ethanol in the presence of a large excess of 4-dimethylaminopyridine (DMAP) afforded in excellent yield $[Ru(DMAP)_6]^{2+}$ instead of the expected *trans*-$Ru(DMAP)_4Cl_2$. This complex is easily isolated as the chloride salt by addition of diethyl ether, and the resulting solid is indefinitely stable provided that exposure to moisture is avoided.

In water, $[Ru(DMAP)_6]^{2+}$ reacts to give an intense purple solution. This reaction is completed in 3 h at 40 °C. The presence of isosbestic points (Figure 1) in its spectroscopic evolution indicates that the reaction proceeds without accumulation of an intermediate. We assign this process to the following consecutive reactions,

$$[Ru(DMAP)_6]^{2+} + H_2O \rightarrow [Ru(DMAP)_5(H_2O)]^{2+} + DMAP, \quad \text{ligand substitution} \quad (1)$$

$$[Ru(DMAP)_5(H_2O)]^{2+} \rightarrow [Ru(DMAP)_5(OH)]^{2+} + H^+, \quad \text{rapid air oxidation with proton loss} \quad (2)$$

The final Ru(III) hydroxo species can be easily isolated as the perchlorate, hexafluorophosphate, or chloride salt. This compound presents a rich chemistry (Scheme 1). For example, its reduction with amalgamated zinc in anaerobic conditions affords the labile Ru(II) aquo species, $[Ru(DMAP)_5(H_2O)]^{2+}$ which in the presence of a 10-fold excess of ligand affords the corresponding $[Ru^{II}(DMAP)_5L]^{n+}$ complex in solution with retention of the $\{Ru^{II}(DMAP)_5\}$ motif.

Scheme 1. Synthesis of all the compounds described in this work

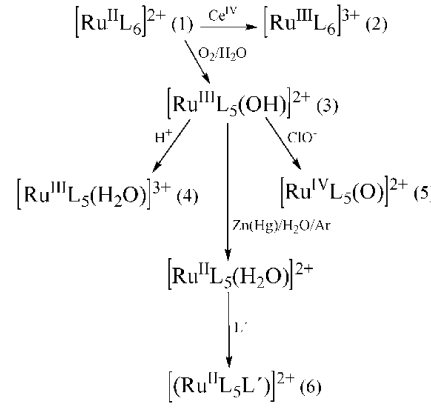

$$[Ru(DMAP)_5(OH)]^{2+} + H^+ \xrightarrow{Zn(Hg)} [Ru(DMAP)_5(H_2O)]^{2+} \quad (3)$$

$$[Ru(DMAP)_5(H_2O)]^{2+} + L \rightarrow [Ru(DMAP)_5L]^{2+} + H_2O \quad (4)$$

The $[Ru(DMAP)_5(Mepz)]^{3+}$ complex can be isolated as the hexafluorophosphate salt, and its structure was confirmed by its NMR spectrum. In contrast, complexes bearing other ligands have proven to be unstable toward ligand loss and oxidation as solids, although they are stable in solution in the presence of an excess of ligand.

Protonation of the coordinated pyrazine in $[Ru(DMAP)_5pz]^{2+}$ takes place between pH 0.0–3.0 as can be inferred from the spectral changes observed in the UV–vis region (see Supporting Information Figure 1). Least-squares fit of these spectra using the following expression:

$$A_t = \frac{\varepsilon_{RupzH^+}[Ru]_t}{1 + \frac{K_a}{[H^+]}} + \frac{\varepsilon_{Rupz}[Ru]_t}{1 + \frac{[H^+]}{K_a}}$$

affords the K_a value for this reaction. The obtained value of 1.3×10^{-1} corresponds to a pK_a of 0.9.

In acid media, protonation of $[Ru(DMAP)_5(OH)]^{2+}$ yields the aquo species $[Ru(DMAP)_5(H_2O)]^{3+}$, which can be isolated as a stable perchlorate or hexafluorophosphate salt. The electronic spectra in solutions of different pH (see Supporting Information Figure 2) provide evidence of the acid–base equilibrium between the aqua and hydroxo species and allows the determination of K_a. The calculated value of $K_a = 1.3 \times 10^{-5}$ corresponds to a pK_a value of 4.9. Titration of the acid–base equivalents of the $[Ru(DMAP)_5(OH)]^{2+}$ confirms the monoprotic nature of this reaction.

Oxidation of $[Ru(DMAP)_5(OH)]^{2+}$ by an hypochlorite aqueous solution (see Supporting Information Figure 3) affords quantitatively the Ru(IV) species which, from all our spectroscopic and electrochemical evidence, can be formulated as the Ru(IV)oxo compound, $[Ru(DMAP)_5O]^{2+}$. The

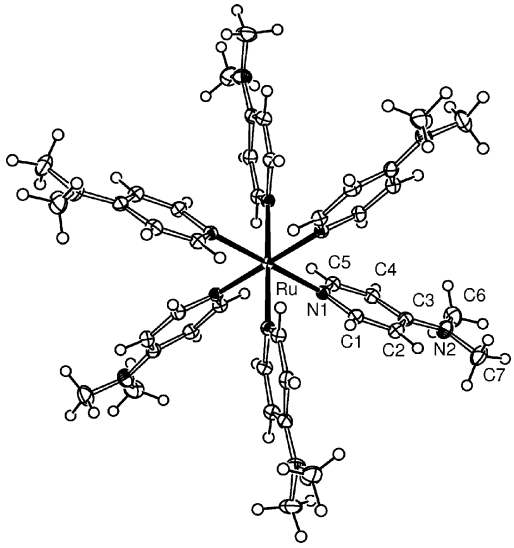

Figure 2. Projection down the crystallographic 3-bar axis of the ruthenium complex in the $[Ru(DMAP)_6]Cl_2 \cdot 6CH_3CH_2OH$ solid showing the labeling of the non-H atoms and their displacement ellipsoids at the 50% probability level. Ru−N bonds are indicated by full lines.

Table 2. Bond Distances (Å) and Angles (deg) around Ruthenium(II) Ion in $[Ru(DMAP)_6]Cl_2 \cdot 6CH_3CH_2OH$

Bond Distances	
Ru−N(1)	2.131(1)
Bond Angles[a]	
N(1)−Ru−N(1′)	95.70(5)
N(1)−Ru−N(1″)	84.30(5)

[a] N(1′) and N(1″) atoms are related to N(1) through the symmetry operations $-y, x - y, z$ and $x - y, x, -z + 1$, respectively.

presence of the Ru^{IV}═O moiety is confirmed by the IR absorption peak at 812 cm^{-1} that we assign as the Ru−O stretch. By precipitation with perchlorate, this Ru oxo compound can be isolated as a solid which remains stable only for a few hours in spite of storing it at 0 °C under argon atmosphere. The magnetic moment at room temperature of this compound (3.09 μ_B) is compatible with a spin S = 1 (expected spin-only contribution equal to 2.83 μ_B with $g = g_e$) arising from a $d_{xy}^2\ d_{xz}^1\ d_{yz}^1$ ground-state configuration, with the *z*-axis along the Ru−O bond direction. This complex shows the expected reactivity of an Ru(IV) species toward organic substrates. The spectral evolution of the dichloromethane solution of $[Ru(DMAP)_5O]^{2+}$ after the addition of a few drops of benzylic alcohol shows the reduction of the Ru(IV) to Ru(II) and indicates the behavior of the ruthenium oxo complex as an oxidant (Supporting Information Figure 4).

Structural X-ray Diffraction Results. Figure 2 is a molecular plot of the complex drawn with ORTEP.[16] Bond distances and angles around the ruthenium ion are in Table 2.

The ruthenium(II) ion is sited on a crystallographic rotation-inversion 3-bar (S_6) axis of the trigonal $R\bar{3}$ space group and bound to the 4-dimethylaminopyridine (DMAP) ligand through the pyridine N-atom at a distance of 2.131(1) Å. This Ru−N bond length agrees with other determinations in DMAP-containing ruthenium complexes.[17] The ligand is nearly planar [rms deviation of atoms from the mean lest-squares plane of 0.028 Å] with the metal ion laying slightly off the plane [at 0.476 Å]. When comparing with the unbound DMAP molecule,[18] it can be appreciated that upon coordination to Ru(II) ion there are a slight lengthening of about 0.02 Å in the pyridine N−C bond distances [1.359(2) and 1.361(2) Å].

The $[Ru(DMAP)_6]^{2+}$ ion shows a strikingly regular conformation. The six 3-bar (S_6) symmetry operations applied to the independent Ru-DMAP group generate the hexacoordinated $Ru(DMAP)_6$ complex where the metal ion is at the center of an octahedron conformed by the bound-to-metal nitrogen atoms (see Figure 2). As seen down, the octahedron C_3 axis coincident with the crystallographic 3-bar axis, the complex exhibits a paddlewheel-like conformation where the metal is coordinated by six DMAP ligands, alternatively arranged around the axis.

The chlorine ion is sited on a crystallographic 3-fold axis acting as acceptor of EtOH···Cl bonds [d(O···Cl) = 3.112 Å, ∠(O−H···Cl) = 169.46°] with three symmetry related ethanol molecules.

Electrochemistry. Table 3 collects the electrochemical properties of the complexes reported in this article. Cyclic voltammetry of $[Ru(DMAP)_6]^{2+}$ in acetonitrile showed one reversible anodic process with an $E_{1/2}$ value of 0.48 V, corresponding to the Ru(III)/Ru(II) couple. The same result is obtained for the CV experiment with $[Ru(DMAP)_6]^{3+}$ hence confirming its formulation as a one-electron oxidized species. The same behavior is observed for the $[Ru(DMAP)_5L]^{2+/3+}$ (L = pz/$Mepz^+$) complexes in acetonitrile solution, with $E_{1/2}$ values of 0.72 and 0.97 V, respectively. In addition, for the case of the $Mepz^+$-containing complex, one reversible (−0.42 V) and a second irreversible (−1.42 V) reduction waves were observed which are typical of the coordinated $Mepz^+$ ligand. For all these complexes, an ∼200 mV anodic shift is observed for the Ru(III)/Ru(II) $E°$ values in water with respect to acetonitrile.

For the $[Ru(DMAP)_5(OH)]^{2+}$ species two consecutive reversible anodic processes are found in water solution whose $E_{1/2}$ values are strongly pH dependent (Figure 3a). These correspond to the Ru(III)/Ru(II) and Ru(IV)/Ru(III) redox processes. The first oxidation process is reversible, but the second becomes increasingly irreversible at higher pH. The pH dependence of these couples is reported in the Pourbaix diagram showed in Figure 3b. The observed values for the plot slopes agree with our formulation of the involved species.

UV–vis Spectroelectrochemistry of $[Ru(DMAP)_5(OH)]^{2+}$ and Related Species. Spectroelectrochemistry measurements of oxidation of $[Ru(DMAP)_5(OH)]^{2+}$ at pH 7.5 showed a clean conversion from the Ru(III) hydroxo compound to the $[Ru^{IV}(DMAP)_5(O)]^{2+}$ species characterized by the loss of the band at 19.7 × 10^3 cm^{-1} (507 nm) and the

(16) Johnson, C. K. *ORTEP-II. A Fortran Thermal-Ellipsoid Plot Program*; Report ORNL-5318, Oak Ridge National Laboratory: Tennessee, 1976.

(17) (a) Bonnet, S.; Collin, J. P.; Gruber, N.; Sauvage, J. P.; Schofield, E. R. *Dalton Trans.* **2003**, 4654. (b) Chen, J. L.; Zhang, L. Y.; Chen, Z. N.; Gao, L. B.; Abe, M.; Sasaki, Y. *Inorg. Chem.* **2004**, *43*, 1481. (c) Liu, X. X.; Wong, W. T. *Polyhedron* **2000**, *19*, 7. (d) Zong, R. F.; Thummel, R. P. *J. Amer. Chem. Soc.* **2004**, *126*, 10800.

Table 3. Spectroscopic and Electrochemical Data for the Reported Complexes

complex	solvent	$\nu_{max}/10^3$ cm^{-1} ($\varepsilon/10^3$ M^{-1} cm^{-1})	assignment	$E_{1/2}$, V (ΔE_p, mV)
$[Ru(DMAP)_6]^{2+}$	water	28.4 (45.5)	dπ Ru$-\pi^*$ DMAP	
	acetonitrile	27.9 (38.8)	dπ Ru$-\pi^*$ DMAP	0.48 (80)
$[Ru(DMAP)_5(H_2O)]^{2+}$	water	28.7 (19.1)	dπ Ru$-\pi^*$ DMAP	
$[Ru(DMAP)_5pz]^{2+}$	water	30.4 (33.6)	dπ Ru$-\pi^*$ DMAP	0.41 (130)
		21.1(8.0)	dπ Ru$-\pi^*$ pz	
	acetonitrile			0.72 (100)[a]
$[Ru(DMAP)_5(pzH)]^{3+}$	water	16.9 (11.1)	dπ Ru$-\pi^*$ pzH$^+$	
$[Ru(DMAP)_5Mepz]^{3+}$	water	34.0 (57.9)	dπ Ru$-\pi^*$ DMAP	0.68 (100)
		16.7 (10.8)	dπ Ru$-\pi^*$ Mepz$^+$	
	acetonitrile	16.8 (11.4)	dπ Ru$-\pi^*$ Mepz$^+$	0.97 (80)
				$-$0.42 (80)
				$-$1.42 irr
$[Ru(DMAP)_6]^{3+}$	water	14.2 (11.8)	π^* DMAP$-$dπ Ru	0.24 (130)
		15.9 (7.3)	π^* DMAP$-$dπ Ru	
	acetonitrile	14.2 (13.6)	π^* DMAP$-$dπ Ru	0.48 (80)
		16.1 (7.6)	π^* DMAP$-$dπ Ru	
$[Ru(DMAP)_5(OH)]^{2+}$	water	19.7(6.7)	π^* DMAP$-$dπ Ru	$-$0.04 (90)
				0.39 (330)
	acetonitrile	21.1 (3.6)	π^* DMAP$-$dπ Ru	
$[Ru(DMAP)_5(H_2O)]^{3+}$	water	14.5 (10.2)	π^* DMAP$-$dπ Ru	0.10 (80)
		16.5 (4.5)	π^* DMAP$-$dπ Ru	0.78 (150)
	acetonitrile	15.8 (4.6)	π^* DMAP$-$dπ Ru	
		17.7 (4.4)	π^* DMAP$-$dπ Ru	
$[Ru(DMAP)_5(O)]^{2+}$	water	23.1 (6.2)	π^* DMAP$-$dπ Ru	

[a] The electrochemistry was measured in the presence of an excess of pyrazine to avoid decomposition.

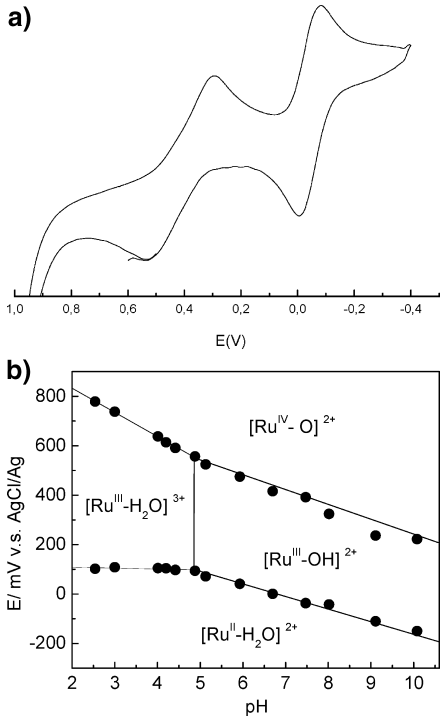

Figure 3. (a) Cyclic voltammogram of $[Ru(DMAP)_5OH]^{2+}$ at pH 8.0. (b) Speciation diagram of the aqueous redox species of $Ru(DMAP)_5L$ moiety, L = H_2O, OH, O.

rise of a new one at 23.3 $\times$ 10^3 cm^{-1} (430 nm) (Figure 4a). Exhaustive reduction fully recovers the starting Ru(III) spectrum. Reduction of the Ru(III) species at pH 2.5 in phosphate buffer solution showed the conversion to the Ru(II) aqua species as inferred from the disappearance of the bands in the visible region and the appearance of a new intense band in the UV region (Figure 4b). Full recovery of the initial Ru(III) species is again observed by exhaustive oxidation of the Ru(II) species. Oxidation of the Ru(III) species at pH 2.5 was not observed due to the solvent discharge at the electrode.

UV–vis Spectroscopy. The spectroscopic data collected for all the reported complexes is listed in Table 3. All the complexes with the ruthenium center in the formal oxidation state (II) show an electronic spectrum with an intense set of bands in the UV region (Figure 5a). The band appearing between 28.0 and 34.0 $\times$ 10^3 cm^{-1}, depending on the identity of the sixth ligand, corresponds to the metal-to-ligand charge transfer MLCT dπ Ru(II) $\rightarrow$ π^* DMAP transition. For the complexes with pyrazine and *N*-methylpyrazinium ligands, another red-shifted intense band is observed in the visible region of the spectrum in water solution at 21.1 and 16.7 $\times$ 10^3 cm^{-1} for $[Ru(DMAP)_5pz]^{2+}$ and $[Ru(DMAP)_5Mepz]^{3+}$, respectively. These bands correspond to the MLCT dπ Ru(II) $\rightarrow$ π^* pz and dπ Ru(II) $\rightarrow$ π^* Mepz$^+$. In the case of compound $[Ru(DMAP)_5Mepz]^{3+}$, an additional weak band (extinction ε of ca. 400 M^{-1} cm^{-1}) is observed at lower energies (ca. 12.0 $\times$ 10^3 cm^{-1}) in water and acetonitrile solutions. This band is also observed in the $\{Ru^{II}(NH_3)_5\}$ analogue spectrum.[19]

The $[Ru^{III}(DMAP)_6]^{3+}$ complex exhibits a completely different electronic spectrum (Figure 5b). The set of overlapped bands appearing in the visible region between 14.0 and 16.0 $\times$ 10^3 cm^{-1}, correspond to LMCT transitions, of π DMAP $\rightarrow$ dπ Ru(III) character. Another set of bands, presumably LMCT, can be distinguished in the UV (27.0–29.0 $\times$ 10^3 cm^{-1}) but appear masked by the intense intraligand CT bands of the DMAP ligand. The other Ru(III) com-

(18) (a) Biradha, K.; Edwards, R. E.; Foulds, G. J.; Robinson, W. T.; Desiraju, G. R. *J. Chem. Soc., Chem. Commun.* **1995**, 1705. (b) Ohms, U.; Guth, H. *Z. Kristallogr.* **1984**, *166*, 213.

(19) Creutz, C.; Chou, M. H. *Inorg. Chem.* **1987**, *26*, 2995.

(20) Albores, P.; Rossi, M. B.; Baraldo, L. M.; Slep, L. D. *Inorg. Chem.* **2006**, *45*, 10595.

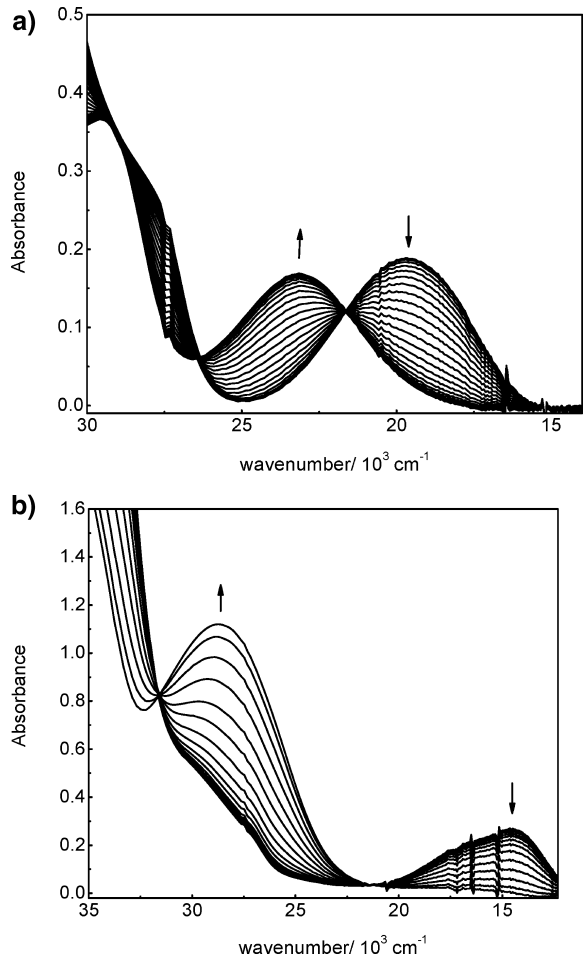

Figure 4. (a) OTTLE spectroelectrochemical oxidation of $[Ru(DMAP)_5(OH)]^{2+}$ in water at pH 7.5. Arrows show appearing and disappearing of product and reactants bands. (b) OTTLE spectroelectrochemical reduction of $[Ru(DMAP)_5(OH)]^{2+}$ in water at pH 2.5. Arrows show appearing and disappearing of product and reactants bands.

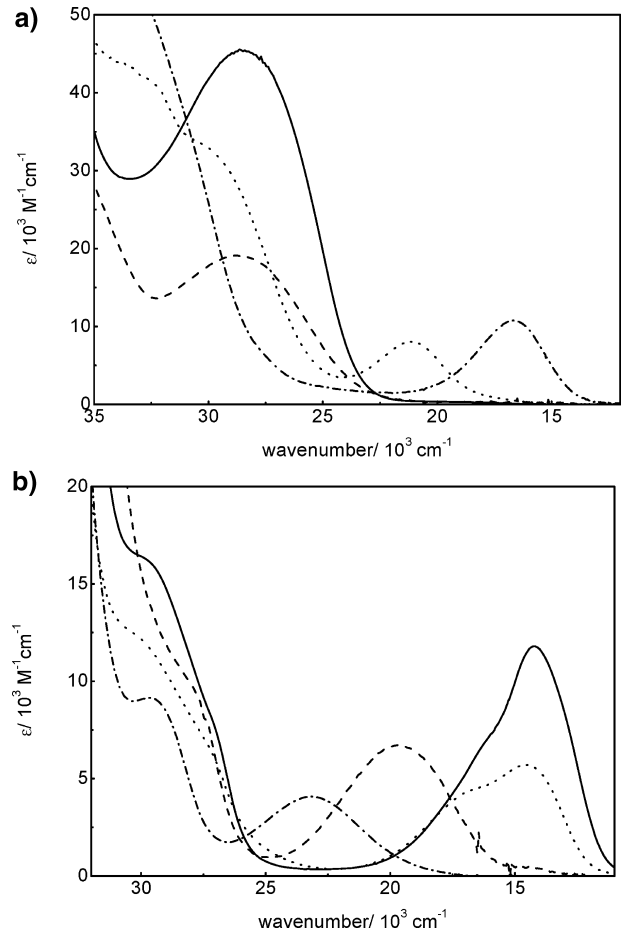

Figure 5. (a) UV–vis spectra in water of complexes $[Ru(DMAP)_6]^{2+}$ (—), $[Ru(DMAP)_5H_2O]^{2+}$(---), $[Ru(DMAP)_5pz]^{2+}$ (•••), and $[Ru(DMAP)_5Mepz]^{3+}$ (-•-). (b) UV–vis spectra in water of complexes $[Ru(DMAP)_6]^{3+}$ (—), $[Ru(DMAP)_5H_2O]^{3+}$ (•••), $[Ru(DMAP)_5OH]^{2+}$, (- -), and $[Ru(DMAP)_5O]^{2+}$ (-•-).

pounds, namely $[Ru(DMAP)_5(OH)]^{2+}$ and $[Ru(DMAP)_5(H_2O)]^{3+}$, also exhibit in the visible region of their spectra a set of bands corresponding to LMCT π DMAP $\rightarrow$ dπ Ru(III) transitions, but with remarkably lower intensity. The oxo Ru(IV) species presents an electronic spectrum that resembles the one of the hydroxo Ru(III) compound but now with the LMCT band blue-shifted with respect to the latter.

DFT Calculations. By means of DFT calculations, we obtained vacuum optimized geometries for the complexes reported in this work. Some representative conformations are available in Supporting Information Figure 5, while relevant calculated distances are listed in Table 4. For all the complexes, the paddlewheel-like configuration adopted by the DMAP ligands is well reproduced theoretically except for the $[Ru(DMAP)_6]^{2+/3+}$ compounds where the tilt angle is almost zero. The pseudo octahedral environment is also well-reproduced with calculated angles close to 90° in all cases.

The frequencies of IR-active modes were calculated for complexes $[Ru(DMAP)_5(OH)]^{2+}$ and $Ru(DMAP)_5(O)]^{2+}$. A closely linear correlation is observed between calculated and experimental frequencies (see Supporting Information Figure 6).

TD-DFT calculations performed for all the complexes afforded theoretical energies for the vertical transitions to the excited states expected to occur in the electronic spectra. The major MO contributions of these excited state's CI determinants, along with the corresponding oscillator strengths, were analyzed to assign the origin of the transitions. These results are summarized in Table 5.

Mulliken−Hush Two-States Analysis of the CT Spectroscopy for $[Ru(DMAP)_5L]^{n+}$, L = pz and Mepz$^+$. To evaluate the M−L mixing degree in these two complexes, we performed a two-states Mulliken−Hush (M−H) type treatment of the measured UV–vis spectra, following a procedure recently reported by us.[20] We chose the two adiabatic states localized over the $\{Ru^{II}(DMAP)_5\}$ moiety and the L ligand with the Hamiltonian,

$$H(q_1) = \begin{pmatrix} \lambda_1 {q_1}^2 & H_{ML} \\ H_{ML} & \Delta G^\circ + \lambda_2 (q_1 - 1)^2 \end{pmatrix}$$

$$\mu^D = \begin{pmatrix} 0 & 0 \\ 0 & e r_{12} \end{pmatrix}$$

We set the r_{12} distance equal to the M−L distance derived from the DFT geometry optimizations, adopting the geometrical center of the L ligand aromatic ring as the L

Table 4. Selected Bond Distances from the DFT at the B3LYP Level Geometry Optimizations.

	optimized distances (Å)		
compound	$Ru-N_{eq}$	$Ru-N_{ax}$	Ru−O
$[Ru(DMAP)_5(H_2O)]^{3+}$	2.139 2.139 2.149 2.149	2.056	2.167
$[Ru(DMAP)_5(OH)]^{2+}$	2.134 2.138 2.147 2.171	2.167	1.970
$[Ru(DMAP)_5(O)]^{2+}$	2.139 2.139 2.153 2.153	2.273	1.801
		Ru−N	
$[Ru(DMAP)_6]^{2+}$		2.182 2.182 2.182 2.183 2.183 2.183	
		Ru−N	
$[Ru(DMAP)_6]^{3+}$		2.160 2.160 2.162 2.163 2.169 2.169	
	$Ru-N_{eq}$	$Ru-N_{ax}$	$Ru-N_L$
$[Ru(DMAP)_5(pz)]^{2+}$	2.187 2.188 2.188 2.189	2.171	2.126
$[Ru(DMAP)_5(Mepz)]^{3+}$	2.175 2.177 2.196 2.197	2.170	2.022
	$Ru-N_{eq}$	$Ru-N_{ax}$	Ru−O
$[Ru(DMAP)_5(H_2O)]^{2+}$	2.148 2.148 2.149 2.151	2.116	2.223

electronic density centroid. We also constrained the λ_1 value to be the same for both compounds, as they share essentially identical adiabatic ground states localized on the $\{Ru^{II}(DMAP)_5\}$ moiety. The obtained simulated spectra are shown in Figure 6, while the relevant parameters describing the M−L coupling are listed in Table 6.

Discussion

Chemistry of the $[Ru(DMAP)_6]^{2+}$ Cation in Aqueous Solution. Previous reports of the reaction of *trans*-$Ru(DMSO)_4Cl_2$ with substituted pyridines point to *trans*-$Ru(L)_4Cl_2$ as the only product.[5,6] The preparation of $[Ru(py)_6]^{2+}$ [7] does not involve the direct reaction of pyridine with a ruthenium starting material. In fact, no successful reactions of *trans*-$Ru(py)_4Cl_2$ with neutral ligands are known. However, the basic ($pK_a \sim 9.7$) 4-dimethylaminopyridine ligand does succeed in fully substituting *trans*-$Ru(DMSO)_4Cl_2$ to give the high symmetric $[Ru(DMAP)_6]^{2+}$ complex. This result could most probably be ascribed to the increased electron-donor capability of the DMAP ligand making the hypothetical *trans*-$Ru(DMAP)_4Cl_2$ intermediate very labile and in consequence capable of further ligand substitution. The structure of the $[Ru(DMAP)_6]^{2+}$ cation does not reveal significant differences with that observed for the related complexes $[Ru(py)_6]^{2+}$ and $[Ru(NH_3)_6]^{2+}$.[7,21] For example, the mean Ru−N distance of 2.13 Å in the DMAP compound is almost identical to the observed in the hexapyridine (2.12 Å) and in the hexammine complexes (2.14 Å).

One of the most interesting features of this DMAP−ruthenium compound is, undoubtedly, its reaction with water in the presence of oxygen to afford $[Ru^{III}(DMAP)_5(OH)]^{2+}$. This reaction proceeds smoothly, and it is the key step for the preparation of $[Ru(DMAP)_5L]^{n+}$ compounds. This synthetic precursor closely resembles the widely used $[Ru(NH_3)_5Cl]^{2+}$ complex, and our synthetic approach emulates the one reported for the synthesis of the $[Ru(NH_3)_5L]^{n+}$ family of compounds.[8] One crucial difference between these two fragments is the bulky nature of the DMAP ligand, which prevents stabilization of μ-oxo Ru complexes and hence avoids the formation of "Ruthenium Red" like compounds in aqueous media.[22] For this reason, substitution reactions in water solution proceed cleanly. The reduction of the Ru(III) hydroxo compound with Zn(Hg) gives easy access to the labile Ru(II) aqua complex and to a family of $[Ru(DMAP)_5L]^{n+}$ compounds.

The acid–base properties of the Ru(III) hydroxo compound provide information about the electronic density over the metallic fragment. The pK_a value obtained of 4.7 is slightly higher than that observed for $[Ru(NH_3)_5(H_2O)]^{3+}$, at 4.1,[23] but much higher than that of the polypyridinic compound $[Ru(bpy)_2(py)(OH)]^{2+}$ ($\sim$1[24]). This decrease in the acidity of the Ru(III) aqua complex with respect to the latter compound reflects the more basic nature of the DMAP ligand in comparison with conventional pyridine and 2, 2′-bipyridine ligands.

Oxidation of $[Ru^{III}(DMAP)_5(OH)]^{2+}$ affords the Ru(IV) oxo compound, $[Ru(DMAP)_5O]^{2+}$, as the only product thanks to the steric hindrance exerted by the DMAP rings that precludes the formation of any hydroxo/oxo possible bridged products. So far, we have failed in avoiding decomposition of this solid, being for us still unknown the pathways leading to its reduction to the Ru(III) hydroxo species. In spite of its instability, we have been able to characterize this Ru(IV) oxo complex. The diagnostic infrared Ru=O stretching band in the $[Ru(DMAP)_5O]^{2+}$ compound appears at 812 cm^{-1}, an assignment supported by DFT calculations, despite the presence of an additional peak corresponding to C−H wagging modes which is also observed in the Ru(III) hydroxo complex. (see Supporting Information Figure 6). The value

(21) Stynes, H. C.; Ibers, J. A. *Inorg. Chem.* **1971**, *10*, 2304.
(22) Baumann, J. A.; Meyer, T. J. *Inorg. Chem.* **1980**, *19*, 345.
(23) Kuehn, C. G.; Taube, H. *J. Am. Chem. Soc.* **1976**, *98*, 689.
(24) Binstead, R. A.; Meyer, T. J. *J. Am. Chem. Soc.* **1987**, *109*, 3287.
(25) Aoyagi, K.; Yukawa, Y.; Shimizu, K.; Mukaida, M.; Takeuchi, T.; Kakihana, H. *Bull. Chem. Soc. J.* **1986**, *59*, 1493.
(26) Thompson, M. S.; Meyer, T. J. *J. Am. Chem. Soc.* **1982**, *104*, 4106.

Table 5. TD-DFT Calculations at the B3LYP Level of the Electronic Transitions

complex	observed maxima in water (10^3 cm^{-1})	energy transition (10^3 cm^{-1}; osc strength)	main CI determinant contribution	
$[Ru(DMAP)_6]^{2+}$	28.4 (45.5)	27.4 (0.39)	HOMO, HOMO − 1,2 → LUMO + 1,2,3	dπ Ru → π* DMAP
$[Ru(DMAP)_5(H_2O)]^{2+}$	28.7 (19.1)	28.9 (0.26)	HOMO, HOMO − 1,2 → LUMO + 1–7	dπ Ru → π* DMAP
		28.5 (0.18)		
$[Ru(DMAP)_5pz]^{2+}$	30.4 (33.6)	22.2 (0.19)	HOMO − 2 → LUMO	dπ Ru → π* pz
		28.6 (0.27)	HOMO, HOMO − 1 → LUMO + 2,3,5	dπ Ru → π* DMAP
		29.0 (0.23)	HOMO, HOMO − 1,2 → LUMO + 2,4	
$[Ru(DMAP)_5Mepz]^{3+}$	34.0 (57.9)	22.4 (0.29)	HOMO − 6 → LUMO	dπRu → π* $Mepz^+$
	16.7 (10.8)	32.7 (0.11)	HOMO, HOMO − 1 → LUMO + 3,4,5,7	dπ Ru → π* DMAP
		32.9 (0.14)	HOMO, HOMO − 1,2 → LUMO + 2,3,4,6	
		34.1 (0.10)	HOMO, HOMO − 1 → LUMO + 6,7	
		34.3 (0.28)	HOMO, HOMO − 2 → LUMO + 4,6	
$[Ru(DMAP)_6]^{3+}$	14.2 (11.8)	11.5 (0.08)	HOMO − 5 → LUMO	π DMAP → dπ Ru
	15.9(7.3)	11.6 (0.10)	HOMO − 7 → LUMO	
		11.7 (0.10)	HOMO − 9 → LUMO	
$[Ru(DMAP)_5(OH)]^{2+}$	19.7 (6.7)	20.0 (0.02)	HOMO − 13 → LUMO	π DMAP → dπ Ru
		20.6 (0.08)	HOMO − 9,11 → LUMO	
$[Ru(DMAP)_5(H_2O)]^{3+}$	14.5 (10.2)	9.4 (0.06)	HOMO − 5 → LUMO	π DMAP → dπ Ru
	16.5 (4.5)	9.8 (0.04)	HOMO − 7 → LUMO	
		12.2 (0.06)	HOMO − 1,11 → LUMO	
		13.4 (0.10)	HOMO − 7,9 → LUMO	
$[Ru(DMAP)_5(O)]^{2+}$	23.1 (6.2)	21.1 (0.02)	HOMO − 5 → LUMO	π DMAP → dπ Ru
		22.7 (0.03)	HOMO − 3,9 → LUMO	

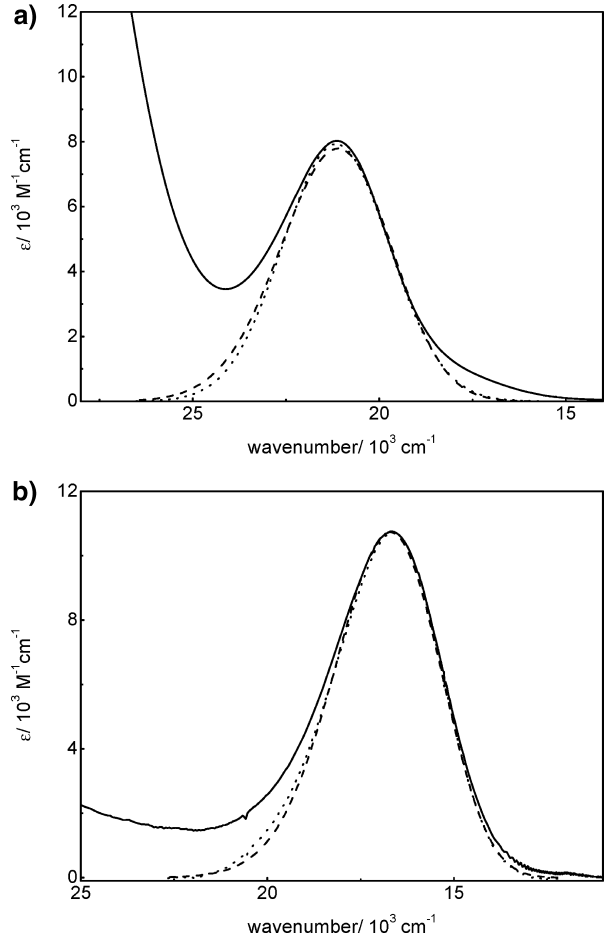

Figure 6. dπ Ru(II) → π* L MLCT band Gaussian deconvolution (•••) of the water experimental spectra (—) for complexes $[Ru(DMAP)_5L]^{2/3+}$, with (a) L = pz and (b) L = $Mepz^+$. The dashed line corresponds to a two-states M−H fitting as described in the text.

of the Ru═O stretching frequency falls in the IR region expected for Ru(IV) oxo compounds. For example, it appears at 805 cm^{-1} in $[RuO(py)_4Cl]^+$ [25] and at 798 cm^{-1} in $[Ru(bpy)_2(py)O]^{2+}$.[26] This Ru(IV) oxo species shows the expected "Ru═O" reactivity[27] as verified preliminary through the positive reaction with benzylic alcohol in a non-coordinating solvent. Its stability in the presence of an excess of oxidant, its solubility in different solvents, and the lability of the Ru(II) aquo species makes it a good candidate as an oxo transfer catalyst.

Table 6. Mulliken−Hush Two-States Metal–Ligand Coupling Parameters for $[Ru(DMAP)_5L]^{n+}$

L	r_{12} (Å)	λ_1 (10^3 cm^{-1})	λ_2 (10^3 cm^{-1})	$\Delta G°$ (10^3 cm^{-1})	H_{ML} (10^3 cm^{-1})	C_M^2
pyrazine	3.5	3.1	4.3	15.5	4.4	0.96
N-methyl pyrazinium	3.5	3.1	4.8	10.6	4.5	0.93

The Pourbaix diagram of these {$Ru(DMAP)_5$} aqua/hydroxo/oxo species clearly demonstrates the existence of the formulated species. The found slopes of ca. 120 and 60 mV/pH for the Ru(IV)/Ru(III) couple in the 2–5 and 5–10 pH range, respectively, are in agreement with the two-proton- and one-proton-coupled redox processes:

$$[Ru(DMAP)_5(O)]^{2+} + 2H^+ + e^- \rightarrow [Ru(DMAP)_5(H_2O)]^{3+}$$

$$[Ru(DMAP)_5O]^{2+} + H^+ + e^- \rightarrow [Ru(DMAP)_5(OH)]^{2+}$$

The almost negligible slope and the 60 mV/pH slope for the Ru(III)/Ru(II) processes in the pH range between 2 and 5 and 5 and 10, respectively, also agree with the no proton and the one-proton-coupled redox processes:

$$[Ru(DMAP)_5(H_2O)]^{3+} + e^- \rightarrow [Ru(DMAP)_5(H_2O)]^{2+}$$

$$[Ru(DMAP)_5(OH)]^{2+} + H^+ + e^- \rightarrow [Ru(DMAP)_5(H_2O)]^{2+}$$

The vertical line that establishes the aqua/hydroxo acid–base equilibrium is in excellent agreement with the obtained pK_a value through spectroscopic measurements.

(27) (a) Dengel, A. C.; Elhendawy, A. M.; Griffith, W. P.; Omahoney, C. A.; Williams, D. J. *J. Chem. Soc., Dalton Trans.* **1990**, 737. (b) Griffith, W. P. *Chem. Soc. Rev.* **1992**, *21*, 179. (c) Roecker, L.; Meyer, J. *J. Am. Chem. Soc.* **1987**, *109*, 746.

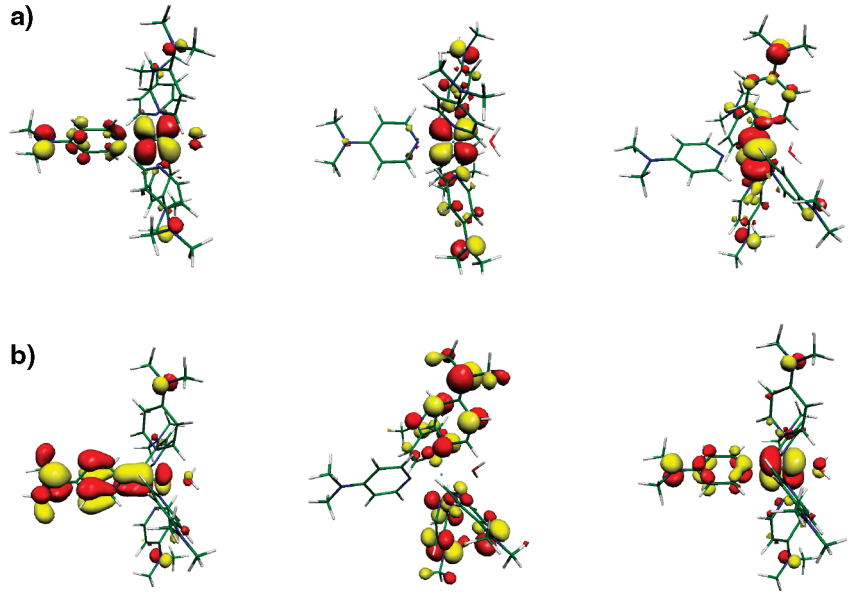

Figure 7. (a) Main molecular orbitals for $[Ru^{II}(DMAP)_5(H_2O)]^{2+}$, as they arise from the DFT calculations at the B3LYP level. (b) Main CI molecular orbitals involved in the DMAP → Ru(III) LMCT bands in the electronic spectrum of $[Ru(DMAP)_5(H_2O)]^{3+}$, as they arise from the TD-DFT calculations at the B3LYP level. (1 and 2) donor DMAP centered orbitals. (3) Ru centered acceptor orbital.

The $E°$ values obtained for these series of complexes can be rationalized in terms of the Lever electrochemical parameters.[28] From the Ru(III)/Ru(II) $E°$ value of $[Ru(DMAP)_6]^{2+}$ in acetonitrile solution, a Lever parameter E_L (V vs NHE as is usual) of 0.11 for DMAP is obtained. This value is clearly smaller than the one for the pyridine (E_L= 0.25) as expected for a more basic ligand. For comparison, the E_L value for ammonia is 0.07, although due to the strong specific interaction of this ligand with solvent, its E_L parameter should be analyzed with caution. The $[Ru(NH_3)_6]^{3+/2+}$ couple $E°$ value of −0.20 V in water solution is one example of the latter behavior.[29] Using the calculated value of E_L for DMAP, $E°$ values of 0.69 and 0.96 V are predicted for the $[Ru(DMAP)_5pz]^{2+}$ and $[Ru(DMAP)_5Mepz]^{3+}$ complexes, respectively, which are in good agreement with the experimentally observed values of 0.72 and 0.97 V.

As it is known, the Lever correlation is not useful for aqua species. However, the predicted value in water for the couple $[Ru(DMAP)_5(H_2O)]^{2+/3+}$ of 0.13 V is in good agreement with the observed $E°$ value of 0.1 V. As expected, the $E°$ value for the Ru(IV) oxo species formation is substantially lower than the one found for other Ru compounds with less basic ligands.[30]

The electronic spectrum of $[Ru(DMAP)_6]^{2+}$ in acetonitrile shows an intense MLCT band, dπ Ru → π* DMAP in origin. The energy of this transition is red-shifted in comparison with that observed in the related $[Ru(py)_6]^{2+}$ (27.9×10^3 vs 29.3×10^3 cm^{-1}) and considerably more intense (38.8×10^3 vs 22.8×10^3 M^{-1} cm^{-1}). These differences can be explained in terms of the enhanced π-donor strength of the DMAP. A simple molecular orbital (MO) analysis shows that the donor orbital involved in the MLCT transition, as obtained from the TD-DFT calculation, includes almost a 30% contribution from the DMAP ligand. As the acceptor orbital also is located on the DMAP ligand, an enhanced intensity is expected.

The spectra of the other Ru(II) compounds reported in this work also present a dπ Ru → π* DMAP transition. The position of this band shifts to higher energies for the less basic ligands. The complexes $[Ru(DMAP)_5pz]^{2+}$ and $[Ru(DMAP)_5Mepz]^{3+}$ show a second MLCT band that involves the dπ Ru → π* L transition. As expected, these bands lie at lower energies. For the Mepz complex, it is considerably red shifted. The protonation of the $[Ru(DMAP)_5pz]^{2+}$ also results in a red shifting of the MLCT band confirming our assignment.

The electronic spectrum of the oxidized species $[Ru(DMAP)_6]^{3+}$ is dominated by the intense set of LMCT bands appearing in the visible, which can be readily assigned to π DMAP → dπ Ru(III) transitions, as confirmed by our DFT results. The hole in the E_g degenerate orbitals acts as the acceptor of this CT transition. Symmetry arguments predict two possible transitions, originated from A_u and E_u orbitals. Similar LMCT transitions from the DMAP ligand have been previously reported for $[Fe^{III}(CN)_5(DMAP)]^{2+}$ and $[Ru^{III}(NH_3)_5(DMAP)]^{3+}$.[16,31]

The remaining Ru(III) compounds also present a set of LMCT bands. For the $Ru^{III}OH_2$ compound, two resolved LMCT bands are observed, but only one for the $Ru^{III}OH$ and $Ru^{IV}O$ species. According to our DFT calculations, the two components of the $[Ru(DMAP)_5(H_2O)]^{3+}$ spectrum correspond to the LMCT transitions whose origin are the axial DMAP (the high energy band) and the equatorial DMAP π donor orbitals (the low energy band, see Figure

(28) Lever, A. B. P. *Inorg. Chem.* **1990**, *29*, 1271.
(29) Endicott, J. F.; Taube, H. *Inorg. Chem.* **1965**, *4*, 437.
(30) Llobet, A.; Doppelt, P.; Meyer, T. J. *Inorg. Chem.* **1988**, *27*, 514.
(31) Shepherd, R. E.; Hoq, M. F.; Hoblack, N.; Johnson, C. R. *Inorg. Chem.* **1984**, *23*, 3249.

5b). The acceptor dπ Ru orbital is the same for both CT components and corresponds to the one that overlaps with the axial DMAP ligand (Figure 7). The single LMCT band observed in the electronic spectra of $[Ru(DMAP)_5(OH)]^{2+}$ and $[Ru(DMAP)_5(O)]^{2+}$ corresponds to these same two LMCT transitions fully overlapped. As expected for these stronger π donor ligands, the energy of the LMCT transition appears shifted to higher energies.

Comparison between the {Ru(DMAP)$_5$} and the {Ru(NH$_3$)$_5$} Fragments. As mentioned above, the reduction of the air-stable $Ru^{III}OH$ compound in the presence of an excess of L gives easy access to a family of $[Ru(DMAP)_5L]^{n+}$ compounds. However, this $\{Ru^{II}(DMAP)_5\}$ fragment appears more reactive than $\{Ru^{II}(NH_3)_5\}$, as rapid ligand dissociation is observed when L excess is suppressed. The extreme acceptor $Mepz^+$ ligand is the only case where the ligand dissociation reaction is precluded, at least in the time scale of hours. Our difficulties to isolate the pyrazine compound as a stable solid, in contrast with $[Ru(NH_3)_5pz]^{2+}$ which could be easily isolated and crystallized,[8] illustrates the high lability of the Ru fragment.

The pK_a of coordinated pyrazine has been used as an evidence of the capacity of the $\{Ru^{II}(NH_3)_5\}$ fragment to transfer electron density from metal to the ligand. The determined pK_a of $[Ru(DMAP)_5(pz)]^{2+}$ (equal to 0.9) is significantly smaller than that observed for the $\{Ru^{II}(NH_3)_5\}$ (2.5[7]) and similar to the free ligand (0.6) indicating a weaker but significant π-interaction between the $\{Ru^{II}(DMAP)_5\}$ and the pyrazine.

The redox potential for reduction of the methylpyrazinium ligand has also been used as an indicator of the extensive π donor capacity of $\{Ru^{II}(NH_3)_5\}$ moiety. The first reduction process for the $[Ru(NH_3)_5Mepz]^{3+}$is observed at -0.71 V, which is even lower than that observed for the free ligand. In contrast, the first reduction process for the $[Ru(DMAP)_5Mepz]^{3+}$ complex is observed at -0.42 V. This value is similar to that observed in other cationic ruthenium complexes[32] and indicates that the back bonding to the methylpyrazinium is less prominent in this complex.

The spectroscopy of the $[Ru(DMAP)_5L]^{n+}$ complexes is also compatible with the bonding picture presented above. The energy of the MLCT band, dπ Ru(II) $\rightarrow \pi^*$ pz, is similar to that observed for $[Ru(NH_3)_5pz]^{2+}$, as expected for a weak π-acceptor like the pyrazine. For $[Ru(DMAP)_5(Mepz)]^{3+}$, the energy of the MLCT band is considerably smaller than that observed for the$[Ru(NH_3)_5(Mepz)]^{3+}$ (16.7×10^3 vs 18.6×10^3 cm^{-1}) indicating again a larger M$-$L mixing degree in the pentammine complex.[19]

For both complexes, L = pz and $Mepz^+$, the band half-widths appear similar to their pentammine equivalent (3200 and 3500 vs 3200 and 4000 cm^{-1}, respectively). As lower ε values are found (13.7×10^3 and 15.0×10^3 M^{-1} cm^{-1} for $[Ru(NH_3)_5L]^{n+}$, L = pz and $Mepz^+$), the integrated intensity of the MLCT bands for the DMAP compounds are lower, suggesting again a diminished mixing between the ligand and the metal orbitals.[19]

These qualitative observations can be rationalized with the combined results obtained from the DFT calculations and the Mulliken$-$Hush two-states treatment. TD-DFT calculations show that the MLCT transitions can be essentially described as promotions between only one pair of molecular orbitals. The H_{ML} values obtained can be compared with the ones reported for the $[Ru(NH_3)_5L]^{n+}$ analogues obtained by an equilibrium geometry Hush analysis.[33] As expected from our previous considerations, lower values are observed for the DMAP compounds (being similar for both L ligands as also observed in the pentammine complexes).

What about the very low intensity second MLCT band observed for the $Mepz^+$ complex? Its origin is undoubtedly the same as for the $\{Ru^{II}(NH_3)_5\}$ analogue assigned by Slep and Olabe,[34] namely, it corresponds to the triplet mixing occurring in the excited-state due to spin–orbit coupling interaction. The intensity ratio between both MLCT bands observed in water for $[Ru(DMAP)_5Mepz]^{3+}$ is 53, a value lower than the corresponding one for the pentammine compound,[35] consistent with a lower M$-$L mixing degree.

Why is the $\{Ru^{II}(DMAP)_5\}$ a weaker π-donor? In this fragment, the dπ orbitals are mixed with the π-orbitals of the DMAP ligands (Figure 7a). This results in a smaller π-electron density over the ruthenium and a smaller overlap with the orbitals of the sixth ligand. The smaller π interaction makes the bond with the sixth ligand weaker hence explaining the observed lability of most of the complexes of this family.

Conclusions

The facile synthesis of the $[Ru(DMAP)_6]^{2+}$ and $[Ru(DMAP)_5(OH)]^{2+}$ compounds and the expected labile behavior of the DMAP ligand make them attractive starting materials for the synthesis of ruthenium compounds bearing an easily oxidable Ru(II) moiety. These compounds could behave as useful building blocks for the preparation of molecular magnetic materials.

Regarding the electronic properties of the $\{Ru^{II}(DMAP)_5\}$ fragment, all the spectroscopic evidence points to a lower M$-$L mixing degree in the compounds $[Ru(DMAP)_5L]^{n+}$, when compared with the exhaustively studied $[Ru(NH_3)_5L]^{n+}$ complexes. The main reason for this behavior can be attributed to the π contribution of the DMAP ligands that competes with the sixth L ligand for the electron density on the Ru center. This contrasting behavior stresses the unique properties of the $\{Ru(NH_3)_5\}$ fragment.

Acknowledgment. The authors thank the University of Buenos Aires, the Consejo Nacional de Investigaciones Científicas y Técnicas (CONICET), and the Agencia para

(32) Coe, B. J.; McDonald, C. I.; Couchman, S. M.; Jeffery, J. C.; Rees, L. H.; Coles, S. J.; Gelbrich, T.; Hursthouse, M. B. *Polyhedron* **2000**, *19*, 1193.

(33) Creutz, C.; Newton, M. D.; Sutin, N. *J. Photochem. Photobiol. A: Chem.* **1994**, *82*, 47.

(34) Slep, L. D.; Olabe, J. A. *J. Am. Chem. Soc.* **2001**, *123*, 7186.

(35) Applying the mathematical procedure described in ref 34 with a fixed ζ Ru = 1200 cm^{-1}, we obtained an $R = 43$ with the following values: $M_L = 5.6 \times 10^3$ cm^{-1}, $H_{ML} = 6.2 \times 10^3$ cm^{-1}, and $C_M^2 = 0.84$.

la Promoción de la Ciencia y la Tecnología (ANPCYT), Argentina, for economic funding and also FAPESP, Brazil. We are also thankful to Johnson Matthey for a generous loan of $RuCl_3$. L.M.B., O.E.P. and P.A. are members of the scientific staff of CONICET. M.B.R. is a graduate fellow of CONICET.

Supporting Information Available: Tables of atomic fractional coordinates and isotropic displacement parameters (Table 1), full intramolecular bond distances and angles (Table 2), atomic anisotropic displacement parameters (Table 3), and hydrogen atoms positions (Table 4); spectrophotometric determination of the-$[Ru(DMAP)_5pz]^{2+}$/$[Ru(DMAP)_5pzH]^{3+}$ equilibrium constant (Figure 1), spectrophotometric determination of the $[Ru(DMAP)_5OH]^{2+}$/$[Ru(DMAP)_5H_2O]^{3+}$ equilibrium constant (Figure 2), UV–vis spectrophotometrical monitoring of oxidation of $[Ru(DMAP)_5(OH)]^{2+}$ in water solution with hypochlorite solution (Figure 3), spectral change of a dichloromethane solution of $[Ru(DMAP)_5O]^{2+}$ upon addition of benzylic alcohol (Figure 4), DFT optimized geometries at the B3LYP level for the complexes reported in this work (Figure 5), DFT infrared frequencies calculated at the B3LYP level for $[Ru(DMAP)_5OH]^{2+}$ and $[Ru(DMAP)_5O]^{2+}$ (Figure 6), cyclic voltammogram of $[Ru(DMAP)_6]^{2+}$ in acetonitrile (Figure 7), and NMR spectrum of $[Ru(DMAP)_6]^{2+}$ in acetonitrile (Figure 8). This material is available free of charge via the Internet at http://pubs.acs.org.

IC7016352